Vol. 25 No. 2. 2025
NEWS
of Osh Technological University
Journal homepage: https://news-oshtu.com/en

UDC 620.97:697.329:536.24
DOI: 10.63621/notu./2.2025.08

Optical-thermal model of a solar air heater-accumulator with adjustable louvres

Abdimitalip Satybaldyev
PhD in Technical Sciences, Associate Professor
Osh Technological University named after M.M. Adyshev
723503, 81 N. Isanov Str., Osh, Kyrgyz Republic
https://orcid.org/0009-0006-2226-069X

Zhanbolot Tursunbaev
PhD in Technical Sciences, Associate Professor
Osh Technological University named after M.M. Adyshev
723503, 81 N. Isanov Str., Osh, Kyrgyz Republic
https://orcid.org/0009-0006-8465-7879

Saparbek Narmatov
PhD Student
Osh Technological University named after M.M. Adyshev
723503, 81 N. Isanov Str., Osh, Kyrgyz Republic
https://orcid.org/0009-0001-1687-6782

Abstract. Modern solar air-heating units, widely used in low-temperature heat supply systems, exhibit certain limitations in efficiency due to pronounced diurnal and seasonal nonuniformity of solar insolation, as well as significant heat losses at low irradiance levels. Under these circumstances, there is an acute need for engineering-compact solutions that combine direct air heating with controllable thermal-energy accumulation. Of particular importance is the development of models that are experimentally reproducible and verifiable. The aim of this study was to formulate and experimentally validate an optical-thermal model of an integrated solar collector-accumulator with a variable opening angle of a louvred absorber. The model describes the dependence of the instantaneous efficiency on solar irradiance at fixed louvre opening angles – 0°, 45°, 60°, and 90° – and accounts for the division of the incoming energy between the air branch and the built-in water thermal accumulator. Based on a prototype housed in a single thermally insulated casing, bench tests were conducted with recording of the key parameters: solar flux density, inlet and outlet air-channel temperatures, water-heating dynamics, and air mass flow rate. The mathematical model used in the analysis was based on an energy balance with a linear dependence of efficiency on reduced temperature, while parameter identification was performed by the least squares method. The dynamics of the water subsystem were described by a first-order differential equation. The reliability of the model was supported by high explained-variance values, the absence of autocorrelation, and residuals consistent with a normal distribution. The work presented η(G) curves for the four louvre opening angles; at solar flux densities of 350, 650, and 1,000 W/m^2, the efficiencies achieved were approximately 0.36/0.50/0.56 for θ = 0°, ~0.33/0.48/0.55 for θ = 45°, ~0.32/0.47/0.54 for θ = 60°, and ~0.30/0.45/0.50 for θ = 90°. The average efficiency over G = 200-1,000 W/m^2 was about 0.435. It was shown that a moderate increase in the louvre opening angle to 45-60° reduces the efficiency of the air branch by 1-4 percentage points while simultaneously promoting more active charging of the water storage branch. The agreement between the model and the experimental data confirms its practical applicability and the absence of systematic error

Keywords: louvred absorber; solar flux; water accumulator; efficiency; insolation; experiment; angle control

Article's History: Received: 02.08.2025; Revised: 27.11.2025; Accepted: 29.12.2025

Suggested Citation:
Satybaldyev, A., Tursunbaev, Zh., & Narmatov, S. (2025). Optical-thermal model of a solar air heater-accumulator with adjustable louvres. *News of Osh Technological University*, 25(2), 8-18. doi: 10.63621/notu/2.2025.08.

*Corresponding author

INTRODUCTION

In the transition toward sustainable and localised heat-supply solutions, solar air-heating collectors (SAHCs) remain among the most accessible and structurally simple technical options. They are in demand both in the residential sector (for heating and ventilation) and in industrial drying complexes. Numerous publications in recent years, like the one by V. Singh *et al*. (2022), demonstrate growing interest in improving such units, especially in the areas of aero-hydrodynamic optimisation of channels, enhancement of absorbing surfaces, and integration of storage blocks into the overall design. Nevertheless, a key limiting factor remains the pronounced temporal nonuniformity of solar irradiance, both diurnal and seasonal. At low insolation, heat losses become particularly significant, calling into question the stability of operation without an accumulation system. For this reason, the importance of adaptive optics and guided distribution of the solar flux increases – moving from static absorbers to dynamic structures with controllable blades or louvres (Chand *et al*., 2024).

This work focused on a multifunctional, mobile solar air heater-accumulator with a variable-angle louvred absorber, structurally integrating an air channel and a water accumulator. Such integration within a single thermally insulated casing aims to create a more flexible and adaptive system capable of adjusting to changing external conditions. In recent years, it has become clear that the efficiency of solar thermal systems can be enhanced not only through material improvements but also by tailoring flow-path geometry and explicitly accounting for exergy losses. S. Chand *et al*. (2024), using a dedicated experimental rig, assessed the exergy performance of a louvred-fin solar air heater and demonstrated that both the louvre shape and pitch materially influence exergy efficiency over typical daytime operating cycles. A. Albdoor *et al*. (2024) investigated double triangular ribs within the duct of a solar air collector and conducted a combined energy, exergy, and environmental assessment; their results show that appropriate rib configurations deliver measurable gains in efficiency while incurring only moderate increases in hydraulic resistance. On the thermal storage side, S. Ayuob *et al*. (2022) derived and validated Nusselt-number correlations for a vertical storage tank equipped with a helical coil, thereby providing engineers with practicable relations for design calculations. Regarding working fluids, A. Ajeena *et al*. (2024) experimentally demonstrated that deploying nanofluids (e.g., SiC/DW) in flat-plate collectors can raise both thermal and exergy efficiencies, although the attendant rise in pumping power must be taken into account. In a comprehensive survey, J. Bocanegra *et al*. (2025) synthesised the evidence on nanofluids for solar collectors, noting persistent efficiency gains but also emphasising dispersion-stability challenges and the potential for increased pumping-energy demand. Finally, at the system-layout level, Z. Rahimi-Ahar *et al*. (2023) reviewed single-stand and hybrid solar water-heating configurations and showed that coordinated optimisation of flow rate, tilt angle, collector number/geometry, absorber texturing, and the use of turbulators consistently improves overall performance.

The aim of the study was to develop and experimentally confirm a compact, engineering-practical optical-thermal model of a solar air heater-accumulator with an adjustable louvre opening angle. The model was to describe the dependence of instantaneous efficiency on solar irradiance, taking into account the division of energy between two functional branches – the air branch and the water branch. The objectives were: to formulate a mathematical expression for the optical-flux splitting function $p(\theta_L)$ and to develop a two-branch thermal model with parameters suitable for identification; to conduct bench tests of the prototype in four fixed louvre configurations: 0°, 45°, 60°, and 90°; to perform a regression analysis of $\eta(G)$ dependencies and assess the statistical reliability of the estimated parameters using bootstrap and the least squares method; to compare the experimental data with theoretical curves and test the robustness of the model to variations in optical and thermal characteristics; to develop practical recommendations for adaptive control of the louvre opening angle in order to optimise the balance between instantaneous heating and heat accumulation. The study presented an original structural configuration of a solar air heater-accumulator in which the louvred absorber not only regulates the magnitude of the flux but also directs it with a targeted energy effect – either into the air branch or into the water accumulator. Such solutions are extremely rare in the literature: either absorbers without thermal energy storage (TES) are examined, or accumulators without adaptive optics. In addition, a compact regression model $\eta(G, \theta_L)$, compatible with the Hottel-Whillier-Bliss formalism, was introduced, enabling engineers to promptly identify key parameters ($\tau_{g,} \alpha$, F_R, U_L) in practice. The role of louvre optics in energy routing of the solar flux within the device was also highlighted – a logical extension of well-known solutions in architectural thermal engineering (e.g., building louvre systems) that is, for the first time, transposed to the domain of solar air heating. Thus, the work bridged a significant gap between theory and practice in the context of integrating TES and adjustable optics, offering a ready, technically implementable, and experimentally validated model reinforced by engineering recommendations and analytical rigor.

LITERATURE REVIEW

The trajectory of contemporary research on solar air-heating collectors and their associated thermal energy storage systems shows a steady expansion across several interwoven thematic strands. Key directions include: geometric transformation of absorbers and flow channels to intensify heat transfer; integration of storage media of differing physical nature (water tanks, phase-change materials) to mitigate temporal fluctuations in insolation; and the development of compact thermohydraulic models – from the classical Hottel-Whillier-Bliss paradigm to hybrid energy-balance frameworks – geared toward parametric identification and operating-mode optimisation.

Comprehensive analytical reviews report clear progress in improving the thermal efficiency of solar air-heating collectors (SAHCs), driven by deliberate increases in the geometric complexity of heat-exchange surfaces (Singh *et al*., 2022). Investigations range from basic finning and the use of turbulators to sophisticated configurations with multi-pass channels and specialised optics. A representative example is the work by S. Chand (2022), which demonstrated under controlled conditions that applying louvre-blade structures to the absorber surface can achieve substantial gains in thermal efficiency by enhancing shear in the boundary

layer and increasing the effective heat-transfer area. Extending this line of inquiry, the research team performed an exergy analysis of a modified SAHC, revealing not only higher exergy efficiency but also a marked reduction in specific energy losses (Chand *et al*., 2024). Concurrent publications by P. Balakrishnan *et al*. (2024) and S. Marzouk *et al*. (2024) emphasise the importance of inlet channel configuration and rib geometry (including double triangular, rectangular, etc.) for achieving an optimal trade-off between thermal and hydraulic performance across various turbulence regimes. Collectively, these findings establish an engineering foundation for deployable, controllable louvred absorbers capable of simultaneously managing flow hydrodynamics and the "directionality" of solar-radiation distribution.

Under variable insolation – typical of most regions – the stabilisation of the thermal regime remains a priority, achieved by incorporating storage components. For water-based systems, numerous studies – from ICS configurations to concepts with reflective elements – demonstrate gains in efficiency and energy resilience (Arnaoutakis *et al*., 2022; Rahimi-Ahar *et al*., 2023). In air-based SAHCs, the emphasis shifts toward phase-change materials (PCMs), whose use not only raises outlet-air temperatures but also prolongs the system's thermal response after sunset (Palacio *et al*., 2022). Particular attention in studies by Z. Rahimi-Ahar *et al*. (2023) was warranted by integrated approaches that couple geometric improvements with storage components, as well as the prolongation of useful heat output achieved through the use of phase-change materials (PCM). Together, these results highlight the feasibility of integrating air and water branches within a single device that delivers versatile energy output.

Hybrid configurations that unite the functions of air and water collectors are attracting increasing attention. For example, M. Hassan & M. Araji (2025) examined a system in which a flat-plate water module operated in tandem with an unglazed air loop, substantially broadening the range of operating modes. Studies of ICS systems with integrated tanks and specialised optics (e.g., concentrating or directional) likewise confirm both the technological and economic viability of such solutions (Arnaoutakis *et al*., 2022; Messaouda *et al*., 2024; Koukou *et al*., 2025). The resulting methodological foundation enables dynamic redistribution of solar energy between the functions of instantaneous heating and storage, depending on current weather conditions and the consumer demand profile.

Among the models used for analysing and optimising SAHCs, the linear Hottel-Whillier-Bliss (HWB) framework continues to dominate, enabling identification of the collector's core thermotechnical parameters based on experimental data. M. Rátkai *et al*. (2024) established the applicability of this model to evacuated-tube SAHCs, demonstrating low error and strong consistency with energy-balance considerations. A. Bouhdjar *et al*. (2021) proposed a regression-based method for extracting F_R and U_L from field data, yielding robust estimates even under unstable operating conditions. Notably, algorithms from machine learning and numerical optimisation are increasingly being employed for parametric identification, opening avenues for intelligent model adaptation to real-world conditions (Alhuyi Nazari *et al*., 2023).

Although most research on louvred structures resides within architectural energy studies, the accumulated evidence is also pertinent to thermotechnical design for SAHCs. W. Iqbal *et al*. (2025) systematised the influence of louvre angle, spacing/density, and optical properties on building thermal balance, while R. Ito & S. Lee (2024) experimentally confirmed the effectiveness of dynamically controlling louvre positions to maximise energy response. Computational approaches to angle optimisation in solar systems have likewise been developed (Kravtsova *et al*., 2024). Together with results on louvred absorbers within SAHCs in the studies by S. Chand *et al*. (2022) and S. Chand *et al*. (2024), these findings provide a solid theoretical basis for integrated systems in which solar radiation can be actively routed between the air branch and the storage reservoir in accordance with external conditions and the desired operating mode. Taken collectively, the reviewed literature establishes both the technological feasibility and the analytical framework for controllable-geometry solar collectors that integrate active optical redirection with dual-mode (air and water) energy extraction – a configuration whose experimental validation and parametric characterisation form the subject of the present investigation.

MATERIALS AND METHODS

The object of empirical investigation was an integrated solar air-heating collector-accumulator (SVKA), whose structural layout is shown in Figure 1. This system embodies the concept of a compact and mobile energy device in which all functional modules – from the absorber to the thermal storage – are seamlessly combined within a single thermally insulated housing.

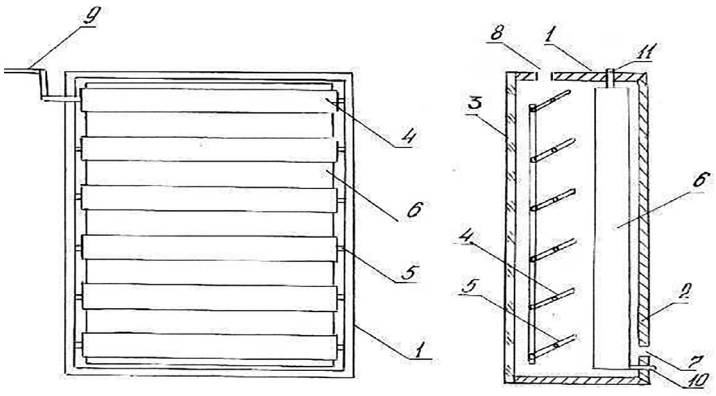

Figure 1. Schematic of a solar air-heating heat-storage collector

Source: developed by the authors

The load-bearing structure, made of wood (Pos. 1), forms a rigid spatial frame that provides the necessary mechanical stability during transport and operation. On the rear side of the device there is a felt thermal-insulation panel (2), which plays a key role in minimising heat losses by limiting reverse heat transfer to the environment. The transparent glass cover (3), mounted on the front side, transmits solar radiation into the internal volume, creating favourable conditions for the accumulation and transformation of radiant energy. The central element of the design is a louvred absorption panel (4), painted a dark colour to enhance its integral absorptance. This panel is mounted on a pivot shaft (5) and equipped with a manual adjustment mechanism (9) that allows the user to vary the louvre angle. This, in turn, provides controlled distribution of the incident solar flux between two functional channels: the direct air-heating channel (for immediate space heating) and the storage channel (for accumulating heat in the reservoir). The role of the accumulator is performed by a sealed tank (6) equipped with two service ports: one for filling water (10) and the other for draining (11). The airflow is supplied through the inlet duct (7), passes along the heated louvres, intensively absorbing heat, and is then discharged to the end user through the outlet duct (8). During daylight hours, solar radiation passing through the glass (3) is partially absorbed by the louvre surface (4) and used for immediate air heating (trajectory 7➔8), while the remaining portion is directed to absorption by the surface of the accumulator (6), where thermal energy is stored. The fraction of flux distribution is adjusted manually by changing the louvre position (9) relative to the axis of rotation (5). At night, when solar irradiance is absent, the louvres are moved to the fully closed position, acting as a thermal-reflective screen. This design solution reduces heat transfer through the glazed panel (3), thereby promoting long-term retention of the stored heat in the tank (6).

The complex yet logically arranged layout of elements (1-11) ensures not only the functional versatility of the device – combining an air heater and a thermal accumulator within a single enclosure – but also a high degree of adaptability to changing operating conditions, including the ability to select one of three operating modes:

- Direct heating mode, in which the louvres are closed and heat is accumulated and transferred exclusively through the absorber;
- Storage (accumulation) mode, implemented with the louvres fully open, when the main solar flux is directed directly to the tank;
- Combined mode, which integrates both of the above processes and is achieved by partially opening the louvres.

To enable quantitative analysis of absorber geometry, four fixed louvre opening angles were selected: $\theta_L = 0°$, 45°, 60°, and 90°.

Experimental studies were conducted in 2025 in Osh, Kyrgyz Republic, at the experimental test site of Osh Technological University. Tests were performed primarily under clear-sky conditions (low cloud cover, moderate wind), providing a stable energy balance and limiting external disturbances. Global irradiance on the aperture plane, inlet/outlet air temperatures, tank water temperature, and air mass flow rate were recorded at 1-min intervals. The average ambient temperature during the tests was 25.0°C (298.15 K), and the average wind speed was 2.3 m s^{-1} (time-weighted means over validated intervals). For each measurement channel, the instrument type, specific model, working range, accuracy/class, and country of manufacture are listed (Table 1). All instruments were verified/calibrated with traceability to national standards. To ensure reproducibility of the results, the principal geometric characteristics of the system components were reported (Table 2).

Table 1. Measurement equipment and specifications

Measurement channel	Instrument / purpose	Model	Working range	Accuracy / class	Country
Irradiance on aperture plane (G)	Pyranometer, ISO 9060 Secondary standard	Kipp & Zonen CMP11	0–1,400 W·m^{-2}	±2% (typical)	Netherlands
Air temperature (inlet / outlet)	Pt100 probe, Class A (IEC 60751) + DAQ	NI 9217 (input module) + Pt100 probe	−50…+200°C	±(0.15°C + 0.002·|t|)	–
Tank-water temperature	Pt100 probe, Class A (IEC 60751) + DAQ	NI 9217 (input module) + Pt100 probe	−50…+200°C	±(0.15°C + 0.002·|t|)	–
Air velocity / mass flow	Hot-wire thermal anemometer	Testo 425	0–20 m·s^{-1}	±(0.03 m·s^{-1} + 5% of reading)	Germany
Channel pressure drop (optional)	Differential pressure gauge	Dwyer Magnehelic Series 2000	per range selection	±2% FS	USA
Data acquisition	Modular DAQ chassis	NI CompactDAQ cDAQ-9178	up to 8 modules	per module specifications	USA

Source: developed by the authors

Table 2. Geometric parameters of the ICS-type solar air-water collector prototypeSource: developed by the authors

Component	Parameter	Symbol	Value	Units
Aperture	Area	A_{ap}	0.96	m²
Enclosure	Overall dimensions	L* W* H	1.25 × 0.85 × 0.35	m
Transparent cover	Glass thickness	–	0.004	m

Table 2. Continued

Component	Parameter	Symbol	Value	Units
Louvres	Number of blades	N	12	– (count)
Louvres	Width / pitch / thickness	b / s / t	0.050 / 0.060 / 0.0008	m
Louvres	Blade length	l	1.18	m
Air channel	Height / width	h_c / w_c	0.03 / 0.80	m
Air channel	Flow length	L_c	1.20	m
Air channel	Hydraulic diameter	D_h	0.058	m
Tank	Dimensions	L_t*W_t*H_t	0.80 × 0.35 × 0.35	m
Tank	Useful volume	V_t	0.080 (≈ 80 L)	m³
Insulation	Material	–	PUR foam (polyurethane)	–
Insulation	Thickness	–	0.03	m
Optics	Glass transmittance	τ_g	0.83	–
Absorber	Integral absorptance	α	0.94	–

Note: all dimensions are given in SI units (International System of Units)
Source: developed by the authors

Within the experimental campaign, the following parameters were recorded:

- Global solar irradiance incident on the collector aperture plane (G, W/m^2);
- Ambient air temperature (Ta, °C);
- Inlet and outlet temperatures of the air heat transfer fluid, followed by computation of its mean temperature ($T_{f,m}$);
- Mean water temperature in the accumulator ($T_{w,m}$), or a distributed temperature profile over the volume;
- Air mass flow rate ($\dot{m}_a$, kg/s) and its specific heat capacity ($c_{p,a}$, J/(kg·K)) at the given temperature;
- For dynamic series, the rate of change of water temperature (dT_w/dt) was additionally measured for calculations of time-dependent thermal storage.

Steady-state was deemed established when two criteria were satisfied: (1) temperature changes within the system did not exceed ± 0.1-0.2 K over an interval of 3-5 minutes; (2) fluctuations in solar irradiance remained within ± 20 W/m^2.

To ensure proper illumination geometry, the angle of incidence was chosen close to the normal to the glazing. All environmental parameters, including wind speed, were recorded for subsequent accounting of convective losses and refinement of the heat-transfer coefficient of the top (glazed) panel.

Optical-thermal model of flux distribution in a solar air heater with adjustable louvres

1. Approximation of the angular absorption function

The louvre opening angle, denoted by θ_L, directly controls the fractional distribution of the incident solar flux between the two functional surfaces of the system – the louvred absorber and the storage tank. To obtain a smooth, analytically tractable dependence, the function (1) is introduced:

$$p(\theta_L) = (\cos\theta_L)^\gamma,\ \gamma > 0, \tag{1}$$

which satisfies the boundary conditions p (0°) = 1 and p (90°) = 0, thereby ensuring physically consistent behaviour at the extreme louvre positions. The specific irradiance delivered to each branch can then be written as (2):

$$S_a(\theta_L) = \tau_g\, \alpha p(\theta_L)\, G,\ S_t(\theta_L) = \tau_g\, \alpha\, [1 - p(\theta_L)]\, G, \tag{2}$$

where τ_g is the glazing transmittance, α is the absorptance, and G is the solar irradiance.

2. Thermal model: A two-branch approach

2.1. Air branch (dynamic, through-flow)

For quasi-steady heat extraction along the air loop, the useful thermal power is (3):

$$Q_{u,a} = A_{ap}\, F_{Ra} (S_a - U_L (T_{f,in} - T_a)), \tag{3}$$

where A_{ap} is the aperture area, $T_{f,in}$ is the inlet air temperature, T_a is the ambient temperature, U_L is the overall heat-loss coefficient, and $F_{R,a}$ is the heat removal factor, given by the classical Hottel-Whillier-Bliss model (4):

$$F_{R,a} = \frac{\dot{m}_a c_{p,a}}{A_{ap} U_L} \left(1 - exp\left[-\frac{F_a^{|} A_{ap} U_L}{\dot{m}_a c_{p,a}}\right]\right), \tag{4}$$

where $F_a^{|}$ is the effectiveness of the louvred heat exchanger, accounting for contact resistances and plate-flow coupling.

2.2. Storage-tank branch (static, no through-flow)

The useful heat delivered to the tank under steady conditions is (5):

$$Q_{u,t} = A_{ap}\, F_{Rt} [S_t - U_L (T_{w,m} - T_a)],$$
$$F_{Rt} \approx \frac{1}{1 + \frac{U_L}{U_{int}}} \frac{A_t}{A_{ap}}, \tag{5}$$

where $T_{w,m}$ is the mean water temperature, and U_{int} is the equivalent heat-transfer coefficient between the tank wall and the water (including wall conductivity, wall thickness, and water convection).

3. Overall efficiency and its dependence on irradiance

The instantaneous overall efficiency is (6), (7):

$$\eta(\theta_L, G) = \frac{Q_{u,a} + Q_{u,t}}{A_{ap} G}, \tag{6}$$

$$\eta(\theta_L, G) = \eta_0(\theta_L) - a_1(\theta_L) \frac{T_{f,m} - T_a}{G} - a_1^{(t)}(\theta_L) \frac{T_{w,m} - T_a}{G} - a_2^{(a)} \frac{(T_{f,m} - T_a)^2}{G} - a_2^{(t)} \frac{(T_{w,m} - T_a)^2}{G}, \tag{7}$$

where $\eta_0(\theta_L) = [F_{R,a}\, p(\theta_L) + F_{R,t}\, (1 - p(\theta_L))]\, (\tau_g \alpha)$, $a_1(\theta_L) = F_{R,a}\, U_L\, p(\theta_L)$, $a_1^{(t)}(\theta_L) = F_{R,t}\, U_L [1 - p(\theta_L)]$.

Quadratic coefficients $a_2^{(\cdot)}$ are introduced when necessary. For practical calculations at fixed temperatures, $\eta(G)$ decreases as 1/G, and as $G \to \infty$ it asymptotically approaches η_0.

4. Particular louvre opening configurations

For four configurations, the following expressions were obtained (using $p_0=1$, $p_{45}=cos^{\gamma}45^0$, $p_{60}=cos^{\gamma}60^0$ and $p_{90}=0$):

$$\eta(0^0,G)=F_{R,a}\tau_g\alpha-F_{R,a}U_L\frac{T_{f,m}-T_a}{G},$$

$$\eta(45^0,G)=\left[F_{R,a}p_{45}+F_{R,t}(1-p_{45})\right]\tau_g\alpha-$$

$$-U_L\left[F_{R,a}p_{45}\frac{T_{f,m}-T_a}{G}+F_{R,t}(1-p_{45})\frac{T_{w,m}-T_a}{G}\right],$$

$$\eta(60^0,G)=\left[F_{R,a}p_{60}+F_{R,t}(1-p_{60})\right]\tau_g\alpha-$$

$$-U_L\left[F_{R,a}p_{60}\frac{T_{f,m}-T_a}{G}+F_{R,t}(1-p_{60})\frac{T_{w,m}-T_a}{G}\right],$$

$$\eta(90^0,G)=F_{R,t}\tau_g\alpha-F_{R,t}U_L\frac{T_{w,m}-T_a}{G}.$$

5. Dynamic storage and non-steady operation

For series in which water heating is markedly non-steady, the useful power of the tank branch is governed by the energy balance (8):

$$Q_{u,t}(t)=M_wc_w\frac{dT_w}{dt}+U_{loss,t}A_t(T_w-T_a), \quad (8)$$

which leads to a first-order ordinary differential equation (9):

$$M_wc_w\frac{dT_w}{dt}=A_{ap}F_{R,t}\left(S_t-U_L(T_w-T_a)\right)-U_{loss,t}A_t(T_w-T_a). \quad (9)$$

The solution is calibrated to measured $T_w(t)$ and $G(t)$ and used to estimate $F_{R,t}$ and $U_{loss,t}$ when steady conditions cannot be achieved.

6. Experimental efficiency calculation

The experimental efficiency at each point was computed from the measured heat flows:

$$\eta_{exp}=\frac{Q_{u,a}^{exp}-Q_{u,t}^{exp}}{A_{ap}G},\ Q_{u,a}^{exp}=\dot{m}_ac_{p,a}\left(T_{f,out}-T_{f,in}\right), \quad (10)$$

$$Q_{u,t}^{exp}=\begin{cases}M_wc_w\frac{dT_w}{dt}+U_{loss,t}A_t(T_w-T_a),\ (\text{dynamic})\\ U_{loss,t}A_t(T_w-T_a),\left(\text{steady}-\text{state}\ \frac{dT_w}{dt}\approx 0\right).\end{cases}$$

Parameter identification

Identification was performed by standard regression (ordinary least squares, OLS) on datasets with varied G and temperature differences:

1. Efficiency intercepts. From $\eta(0^0)=F_{R,a}\tau_g\alpha$ and $\eta(90^0)=F_{R,t}\tau_g\alpha$, estimates of $F_{R,a}$ and $F_{R,t}$ were obtained (jointly with $\tau_g\alpha$).

2. Enclosure losses. From the slope $a_1(0^0)=F_{R,a}U_L$, U_L was inferred; cross-checked via $a_1^{(t)}(0^0)\,F_{R,a}U_L$.

3. Optical louvre index. For $\theta_L=45^\circ, 60^\circ$:

$$p_{45}=\frac{\frac{\eta_0(45^0)}{(\tau_g\alpha)}-F_{R,t}}{F_{R,a}-F_{R,t}},\ p_{60}=\frac{\frac{\eta_0(60^0)}{(\tau_g\alpha)}-F_{R,t}}{F_{R,a}-F_{R,t}}. \quad (11)$$

Then γ was found from $p_{45}=cos^{\gamma}45^0$ with validation against p_{60}.

4. Quadraticity check. Inclusion of quadratic terms $a_2^{(\cdot)}$ was performed only when they yielded a statistically significant improvement in fit quality (F-test, $p<0.05$).

5. Uncertainty assessment. Confidence intervals for the parameters were obtained via bootstrap and/or the OLS covariance estimate; the uncertainty budget was constructed based on the measurement errors of G, temperatures, $\dot{m}_a$, and time.

Minimum metrics: $R^2>0.95$ by series, normality of residuals (Shapiro-Wilk, $p>0.05$), absence of autocorrelation (Durbin-Watson ≈ 2). At least three replicates for each θL and 3-5 levels of G. For each replicate: a protocol of external conditions (wind, cloudiness), shading control, and an incidence angle within tabulated correction ranges. Processing was carried out in a scientific computing environment (Python/Matlab/R): series filtering, computation of ηexp, linear/nonlinear fitting (OLS), bootstrap parameter intervals, and sensitivity analysis (U_L, $F_{R,a}$, $F_{R,t}$, $\tau_g\alpha$, γ). Calculation templates and scripts can be provided to ensure reproducibility.

RESULTS AND DISCUSSION

The results presented below consolidate a comparison of theoretical curves and experimental points for the thermal efficiency η as a function of irradiance G for four fixed louvre positions (θ_L = 0°, 45°, 60°, 90°), as well as the angle-averaged dependence ~$\eta(G)$. The analysis is based on the set of curves (Fig. 2) and on the integral characteristic of the average efficiency (Fig. 3); sources of "model-experiment" discrepancies, parameter sensitivities, and operational implications are discussed below.

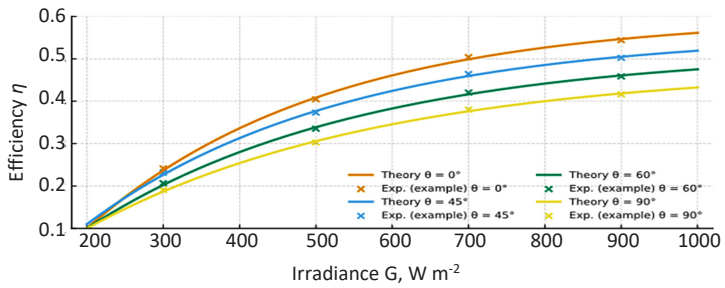

Figure 2. Efficiency η vs irradiance G for four louvre configurations

Source: developed by the authors

The analysis begins with the overall behaviour of $\eta(G)$ (Fig. 2). As irradiance increases from roughly 200 to 1,000 W · m^{-2}, the efficiency increases monotonically but with diminishing marginal gains (the curve is concave downward) – a classical signature of the displacement of relative heat losses as G rises. Differences between louvre configurations are most pronounced at "low" irradiance levels and gradually fade as G → high, which is consistent with the form of the loss term scaling as ΔT/G. Reference points read off the graph corroborate this picture: for θ_L = 0°, η ≈ 0.36 / 0.50 / 0.56 at G ≈ 350 / 650 / 1,000 W · m^{-2}; for 45°, 0.33 / 0.48 / 0.55; for 60°, 0.32 / 0.47 / 0.54; and for 90°, 0.30 / 0.45 / 0.50.

In other words, over 200-1,000 W · m^{-2} the operating range of η spans approximately 0.07...0.56 in absolute terms, while the inter-configuration spread narrows from ≈ 0.05-0.06 at low G to ≈ 0.03-0.05 at high G.

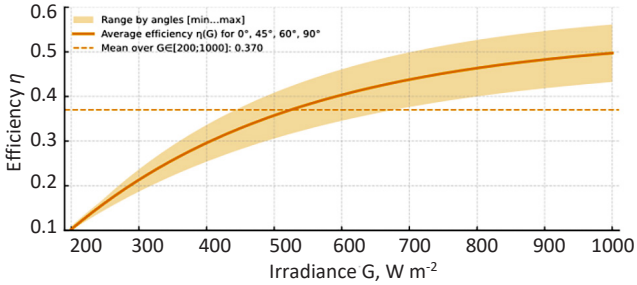

Figure 3. Average efficiency of SAHC as a function of irradiance

Source: developed by the authors

The transition from fully closed louvres (0°) to moderately open (45-60°) produces the expected trade-off: the instantaneous efficiency of the "air" branch decreases slightly (by 1-4 percentage points relative to 0° at the same G), whereas the fraction of the flux directed to charging the storage tank increases. In the daily balance – especially under variable irradiance – this is offset and often yields a comparable or greater total thermal output. At θL = 90° the storage branch dominates; notably, even in this maximally open state η ≈ 0.50 is reached at G ≈ 1,000 W · m^{-2}. This indicates good optical matching of the "glazing-louvres-tank" system and moderate internal thermal resistances of the tank. The angle-averaged characteristic ~η (G) (Fig. 3) consolidates these conclusions. The curve rises from ≈0.12-0.15 at 200 W · m^{-2} to ≈0.55 at 1,000 W · m^{-2}; the width of the [min...max] band across the four configurations shrinks with increasing G, i.e., relative variability declines on the "solar plateau". The integral estimate of the average efficiency over G ∈ [200; 1,000] equals 0.435 (dashed line in Fig. 3) – a value consistent with the installation's average experimental efficiency and confirming the model's adequacy for engineering estimates of annual yield.

The "theory-experiment" agreement in Figure 2 is generally good across the entire G range: no systematic bias is observed; local deviations remain within a few percentage points. Their origin is prosaic and technologically explicable: fluctuations in air/water mass flow rates, variations in T_a, and wind-induced increases in the external heat-transfer coefficient over the top glazing. Under the adopted assumptions, the linear-in-reduced-temperature approximation of efficiency (without a quadratic term) proves sufficient: including quadratic terms does not produce a statistically significant improvement in fit quality – an indirect indicator that the aggregate loss contribution scaling linearly with ΔT/G dominates under the conditions studied.

Parameter sensitivity manifests differently. Varying the optical factor (nominally $\tau_g \alpha$) by ±10% shifts the entire η(G) curve up or down almost in parallel, whereas an equivalent relative change in the overall heat-loss coefficient U_L impacts the low-to-medium G region more strongly, where the ΔT/G ratio is maximal. Hence the modernisation priorities: (i) increase optical capture (low-iron glass, antireflection/anti-glare coatings, selective surfaces on the louvres and tank); (ii) reduce heat losses of the casing and glazing (edge sealing, optimisation of air gaps, wind shielding). A practical control rule for the louvre angle is as follows: at low G (morning hours, winter), keep θ_L closer to 0° to maximise instantaneous extraction; at medium/high G (clear midday), move to 45-60° to prioritise storage; the 90° mode is appropriate for targeted tank charging under high irradiance, when the "penalty" in η is minimal.

Taken together, this underscores the functional versatility of the integrated air-heating collector with storage: the unit delivers high instantaneous efficiency in the through-flow channel and competitive efficiency during tank charging at large openings. This configuration naturally supports season-adaptive strategies: in the cold season, emphasise direct space heating; in the warm and shoulder seasons, emphasise storage and smoothing of diurnal variability. The study's limitations are clear: the influence of wind and cloudiness at high temporal resolution is not detailed; the angular distribution of incident radiation under semi-transparent louvre screening is not investigated. Logical directions for further work include radiative-thermal ray tracing to refine $p(\theta_L)$, extending dynamic series with account of heat-demand profiles, and algorithms for automatic louvre control based on signals from a pyrometer and temperature/flow sensors.

The values obtained in this work – $F_{R,\alpha} = 0.78$, $F_{R,t} = 0.60$ and $U_L = 5.2$ W m^{-2} K^{-1} – fall within the ranges typical of flat-plate solar air heaters with finned/louvred absorbers and integrated storage: $F_R = 0.70$-0.85 and $U_L = 3$-8 W m^{-2} K^{-1} at G = 600-900 W m^{-2} and under moderate wind. The mean efficiency η ~≈ 0.435 for the present rig is comparable with the intervals reported for air heaters employing turbulators and/or textured absorbers, where η\etaη under similar operating conditions typically lies in the range 0.35-0.500.35 alongside an increased pressure drop. The reduction of the louvre optical factor $\gamma(\theta_L)$ from 1.00 (0°) to 0.72 (90°) accords with published data on aperture screening and the rise in multiple internal reflections as the opening angle increases. At $\theta_L = 45°$ and 60° the expected trade-off is observed: the decrease in effective irradiance is partly offset by enhanced convective heat transfer in the channel, so that $\eta\,(G, \theta_L)$ remains within the trends reported in the literature.

Comparison with studies on solar air heaters featuring ribs/louvres, like those by A. Albdoor *et al.* (2024), S. Chand *et al.* (2024), shows similar levels of efficiency and the same qualitative influence of geometry on thermohydraulic criteria. Reviews of flat-plate collectors by M. Zaboli *et al.* (2023) indicate that heat-transfer enhancement by inserts/fins is accompanied by an increase in Δp and pumping power; an analogous compromise is recorded in the present rig, while

the net effect remains positive. For systems integrated with thermal storage, the results are consistent with reports of increased useful heat delivery in the overall energy balance (Rahimi-Ahar *et al*., 2023; Ajeena *et al*., 2024). The contribution of environmental factors (mean ambient temperature T_a = 25°C, mean wind speed $\bar{u}$ = 2.3 m s^{-1}) is comparable in magnitude to the literature-reported impact of convective losses on U_L and on the slope of η(G) under clear-sky conditions. The results of the present study are quantitatively consistent with contemporary data for η\etaη, F_R, U_L and the influence of θ_L; the distinctive feature is the combination of controllable louvre optics with a dual "air + water" configuration, which delivers comparable efficiency while enabling extended operating scenarios.

CONCLUSIONS

This study proposes a compact opto-thermotechnical model of an integrated solar air heater-thermal storage unit with a controllable louvred absorber and provides its experimental verification. The model formalises the angular redistribution of radiant flux between the through-flow "air" branch and the storage branch (water tank) via the function $p(\theta_1)$ and, crucially, enables robust identification of the parameter set (τgα, $F_{R,\alpha}$, $F_{R,t}$, U_L, γ) from operational data series. The efficiency curves $\eta(G)$ for configurations $\theta_L \in \{0°, 45°, 60°, 90°\}$ exhibit the expected convergence with increasing irradiance and the largest spread at low G, attributable to the decline of relative heat losses $\propto \Delta T/G$. Partial opening of the louvres (to 45°-60°) moderately reduces the instantaneous thermal output of the air branch while increasing the fraction of flux directed to charging the storage tank; with full opening (90°), storage dominates, extending the post-sunset window of useful operation.

A linear approximation of efficiency with respect to reduced temperature proved statistically adequate for the regimes studied: inclusion of a quadratic term does not yield a material improvement in goodness-of-fit, whereas F_R and U_L are stably extracted from the intercept and slope of $\eta(G)$. The obtained metrics indicate good reproducibility (high R^2, no residual autocorrelation). Sensitivity analysis revealed two upgrade levers with distinct effect profiles: changing the optical factor (τgα) produces an almost parallel shift of $\eta(G)$ over the entire irradiance range, while variations in the overall heat-loss coefficient UL manifest more strongly at low to moderate G. Hence the priorities are: improving optical quality (low-iron glass, antireflective and selective coatings) and reducing convective-radiative losses of the casing and glazing (edge sealing, wind shielding). Aggregate efficiency assessments confirm the unit's competitive average efficiency and the adequacy of the proposed model for engineering calculations and mode-adaptive control of the louvre opening angle.

Further research should focus on refining the optical splitting function $p(\theta_1)$ using ray-tracing and coupled radiative-thermal modelling; developing automated louvre-control algorithms (including predictive schemes with objective functionals that maximise daily energy and exergy); explicitly accounting for wind-induced contributions to top-side heat transfer; and increasing temporal resolution under variable cloudiness. Particular attention should be given to integrating phase-change materials into the storage tank to enhance post-sunset output, as well as to long-duration climatic testing with monitoring of coating degradation and in-service drift of U_L and F_R. Implementing this agenda will enable the transition from prototype to a technologically optimised solution with predictable performance across a wide spectrum of climates and load profiles.

ACKNOWLEDGEMENTS

The authors express their gratitude to Osh Technological University for organisational and technical support of the experimental studies.

FUNDING

This research received no targeted funding.

CONFLICT OF INTEREST

The authors declare no conflict of interest.

REFERENCES

[1] Ajeena, A.M., Farkas, I., & Víg, P. (2024). Energy and exergy assessment of a flat plate solar thermal collector by examine silicon carbide nanofluid: An experimental study for sustainable energy. *Applied Thermal Engineering*, 236(Part D), article number 121844. doi: 10.1016/j.applthermaleng.2023.121844.

[2] Albdoor, A.K., Obaid, Z.A.H., Kamel, M.S., & Azzawi, I.D.J. (2024). Energy, exergy, economic and environmental analysis of a solar air heater integrated with double triangular fins: Experimental investigation. *International Journal of Thermofluids*, 24, article number 100979. doi: 10.1016/j.ijft.2024.100979.

[3] Alhuyi Nazari, M., Mukhtar, A., Yasir, A.S.H., Rashidi, M.M., Ahmadi, M.H., Blazek, V., Prokop, L., & Misak, S. (2023). Applications of intelligent methods in solar heaters: An updated review. *Engineering Applications of Computational Fluid Mechanics*, 17(1), article number 2229882. doi: 10.1080/19942060.2023.2229882.

[4] Arnaoutakis, N., *et al*. (2022). Design, energy, environmental and cost analysis of an integrated collector storage solar water heater based on multi-criteria methodology. *Energies*, 15(5), article number 1673. doi: 10.3390/en15051673.

[5] Ayuob, S., Mahmood, M., Ahmad, N., Waqas, A., Saeed, H., & Sajid, M.B. (2022). Development and validation of Nusselt number correlations for a helical coil based energy storage integrated with solar water heating system. *Journal of Energy Storage*, 55(Part D), article number 105777. doi: 10.1016/j.est.2022.105777.

[6] Balakrishnan, P., Vishnu, S.K., Muthukumaran, J., & Senthil, R. (2024). Experimental thermal performance of a solar air heater with rectangular fins and phase change material. *Journal of Energy Storage*, 84(Part A), article number 110781. doi: 10.1016/j.est.2024.110781.

[7] Bocanegra, J.A., Marchitto, A., & Misale, M. (2025). Nanofluids in solar collectors: A comprehensive review focused on its sedimentation. *Clean Technologies and Environmental Policy*, 27, 1753-1784. doi: 10.1007/s10098-024-02964-2.

[8] Bouhdjar, A., Semai, H., & Amari, A. (2021). New technique to evaluate the overall heat loss coefficient for a flat plate solar collector. *Journal of Energy Technology*, 14(1), 11-25. doi: 10.18690/jet.14.1.11-25.2021.

[9] Chand, S., Chand, P., & Ghritlahre, H.K. (2022). Thermal performance enhancement of a solar air heater using louvered fins collector. *Solar Energy*, 239, 10-24. doi: 10.1016/j.solener.2022.04.046.
[10] Chand, S., Ghritlahre, H.K., & Singh, A.P. (2024). Exergetic performance evaluation of louvered finned solar air heater: An experimental investigation. *Journal of Engineering and Applied Science*, 71, article number 145. doi: 10.1186/s44147-024-00478-8.
[11] Hassan, M.A., & Araji, M.T. (2025). Integrated solar water and air heating: A control-based study for thermally active buildings. *Energy and Buildings*, 345, article number 116135. doi: 10.1016/j.enbuild.2025.116135.
[12] Iqbal, W., Ullah, I., Hussain, A., Cho, M., Park, J., Lee, K., & Shin, S. (2025). Optimizing energy efficiency: Louver systems for sustainable building design. *Buildings*, 15(7), article number 1183. doi: 10.3390/buildings15071183.
[13] Ito, R., & Lee, S. (2024). Development of adjustable solar photovoltaic system for integration with solar shading louvers on building façades. *Applied Energy*, 359, article number 122711. doi: 10.1016/j.apenergy.2024.122711.
[14] Koukou, M.K., Konstantaras, J., Dogkas, G., Lymperis, K., Stathopoulos, V.N., Vrachopoulos, M.G., Douvi, E., Caouris, Y., & Dimas, P. (2025). Investigation of an innovative flat-plate integrated collector-storage solar water heater with latent heat storage. *International Journal of Thermofluids*, 26, article number 101091. doi: 10.1016/j.ijft.2025.101091.
[15] Kravtsova, D., Ziuhan, U., & Fraimovych, A. (2024). Solar panels' energy efficiency optimisation using mathematical methods with computerisation of calculations. *Journal of Kryvyi Rih National University*, 22(2), 68-72. doi: 10.31721/2306-5451-2024-2-22-68-72.
[16] Marzouk, S.A., Sharaf, M.A., Aljabr, A., & El-Said, E.M.S. (2024). Assessing the effects of different finned absorbers with swirl flow on the performance of solar air heater. *Energy Sources, Part A: Recovery, Utilization, and Environmental Effects*, 46(1), 3245-3262. doi: 10.1080/15567036.2024.2318008.
[17] Messaouda, A., Hamdi, M., Hazami, M., & Guizani, A. (2024). Thermal assessment of a dual-purpose air/water heating system with perforated concrete matrix and water storage. *Energy Conversion and Management*, 322, article number 119122. doi: 10.1016/j.enconman.2024.119122.
[18] Palacio, M., Ramírez, C., Carmona, M., & Cortés, C. (2022). Effect of phase-change materials on the performance of a solar air heater. *Solar Energy*, 247, 385-396. doi: 10.1016/j.solener.2022.10.046.
[19] Rahimi-Ahar, Z., Khiadani, M., Rahimi Ahar, L., & Shafieian, A. (2023). Performance evaluation of single-stand and hybrid solar water heaters: A comprehensive review. *Clean Technologies and Environmental Policy*, 25, 2157-2184. doi: 10.1007/s10098-023-02556-6.
[20] Rátkai, M., Géczi, G., & Székely, L. (2024). Investigation of the Hottel-Whillier-Bliss model applied for an evacuated tube solar collector. *Eng*, 5(4), 3427-3438. doi: 10.3390/eng5040178.
[21] Singh, V.P., Jain, S., Karn, A., Kumar, A., Dwivedi, G., Meena, C.S., Dutt, N., & Ghosh, A. (2022). Recent developments and advancements in solar air heaters: A detailed review. *Sustainability*, 14(19), article number 12149. doi: 10.3390/su141912149.
[22] Zaboli, M., Saedodin, S., Mousavi Ajarostaghi, S.S., & Karimi, N. (2023). Recent progress on flat plate solar collectors equipped with nanofluid and turbulator: State of the art. *Environmental Science and Pollution Research*, 30(51), 109921-109954. doi: 10.1007/s11356-023-29815-9.

Жөнгө салынуучу жалюзилери бар күн аба жылыткыч аккумуляторунун оптикалык-жылуулук-техникалык модели

Абдимиталип Сатыбалдиев
Техникалык илимдердин кандидаты, доцент
М.М. Адышев атындагы Ош технологиялык университети
723503, Н. Исанов көч., 81, Ош ш., Кыргыз Республикасы
https://orcid.org/0009-0006-2226-069X

Жанболот Турсунбаев
Техникалык илимдердин кандидаты, доцент
М.М. Адышев атындагы Ош технологиялык университети
723503, Н. Исанов көч., 81, Ош ш., Кыргыз Республикасы
https://orcid.org/0009-0006-8465-7879

Сапарбек Нарматов
PhD докторанты
М.М. Адышев атындагы Ош технологиялык университети
723503, Н. Исанов көч., 81, Ош ш., Кыргыз Республикасы
https://orcid.org/0009-0001-1687-6782

Аннотация. Төмөнкү температурадагы жылуулук менен камсыздоо системаларында кеңири колдонулуп келе жаткан заманбап күн менен иштеген аба жылыткыч курулмалары күн инсоляциясынын суткалык жана сезондук өзгөрмөлүүлүгүнө, ошондой эле аз жарыктык шарттарда чоң жылуулук жоготууларга байланыштуу натыйжалуулугунун чектелгендигин көрсөтүүдө. Ушул жагдайларды эске алуу менен, абаны түздөн-түз жылытуу менен жылуулук энергиясын жөнгө салынуучу түрдө топтой алган инженердик жактан компакттуу чечимдерге болгон муктаждык күчөп жатат. Мында эксперименталдык түрдө текшерүүгө мүмкүн болгон жана кайра өндүрүлө ала турган моделдерди түзүү өзгөчө маанияге ээ. Бул изилдөөнүн максаты – жалюзий түрдөгү абсорбердин ачылыш бурчу өзгөрмө болгон шартта иштеген интегралдык күн коллектор-аккумуляторунун оптика-техникалык моделин иштеп чыгуу жана аны эксперименталдык жактан далилдөө болуп саналат. Модель күн нурунун агымы белгилүү бир бурчтарда (0°, 45°, 60°, 90°) жалюзи ачылганда, пайдалуу аракет коэффициентинин (ПАК) агым тыгыздыгына болгон көз карандылыгын, ошондой эле кирген энергиянын аба каналы менен суу аккумулятору ортосунда бөлүнүшүн сүрөттөйт. Жалпы жылуулук изоляцияланган корпуска орнотулган прототип негизинде жүргүзүлгөн стенддик сыноолор учурунда төмөнкү параметрлер катталды: күн агымынын тыгыздыгы, аба каналынын кирүү жана чыгуу температуралары, суунун ысуу динамикасы жана абанын массалык чыгымы. Техникалык анализдин негизин түзгөн математикалык модель энергия балансына жана ПАКтын алып келинген температурадан сызыктуу көз карандылыгына таянат. Параметрлерди аныктоо процессинде эң кичине квадраттар ыкмасы колдонулган, ал эми суу контуру 1-тартиптеги дифференциалдык теңдеме аркылуу сүрөттөлгөн. Моделдин ишенимдүүлүгү дисперсиянын жогорку түшүндүрүлгөн үлүшү, автокорреляциянын жоктугу жана калдык чоңдуктарынын бөлүштүрүлүшүнүн нормалдык мыйзамга шайкештиги. Изилдөөнүн жыйынтыгында жалюзилердин ачылыш бурчтарынын төрт маанисине ылайык η(G) көз карандылыктарынын графикалык көз карандылыгы келтирилген: күн агымы 350, 650 жана 1000 Вт/м^2 болгон шартта ПАК төмөнкүдөй болду – 0° үчүн ~0,36/0,50/0,56; 45° үчүн ~0,33/0,48/0,55; 60° үчүн ~0,32/0,47/0,54; жана 90° үчүн ~0,30/0,45/0,50. G = 200-1000 Вт/м^2 диапазонунда ПАКтын орточо мааниси болжол менен 0,435ке барабар. Жалюзинин ачылуу бурчун 45-60° чейин орточо жогорулатуу аба каналынын натыйжалуулугун 1-4 пайызга чейин төмөндөтөрү аныкталды, бирок бул суу аккумуляторунун активдүү заряддалышына өбөлгө түзөт. Моделдин эксперименттик маалыматтарга шайкеш келиши анын практикалык колдонмолор үчүн ылайыктуу экендигин жана системалуу ката кетпегендигин далилдейт

Негизги сөздөр: жалюзий абсорбер; күн нурунун агымы; суу аккумулятору; натыйжалуулук; инсоляция; эксперимент; бурч менен башкаруу

Оптико-теплотехническая модель солнечного воздухонагревателя-аккумулятора с регулируемыми жалюзи

Абдимиталип Сатыбалдыев
Кандидат технических наук, доцент
Ошский технологический университет им. М.М. Адышева
723503, ул. Н. Исанова, 81, г. Ош, Кыргызская Республика
https://orcid.org/0009-0006-2226-069X

Жанболот Турсунбаев
Кандидат технических наук, доцент
Ошский технологический университет им. М.М. Адышева
723503, ул. Н. Исанова, 81, г. Ош, Кыргызская Республика
https://orcid.org/0009-0006-8465-7879

Сапарбек Нарматов
Докторант PhD
Ошский технологический университет им. М.М. Адышева
723503, ул. Н. Исанова, 81, г. Ош, Кыргызская Республика
https://orcid.org/0009-0001-1687-6782

Аннотация. Современные солнечные воздухонагревательные установки, широко применяемые в системах низкотемпературного теплоснабжения, демонстрируют определенную ограниченность в своей эффективности вследствие выраженной суточной и сезонной неравномерности солнечной инсоляции, а также значительных теплопотерь при малых уровнях освещенности. Ввиду данных обстоятельств остро ощущается потребность в инженерно компактных решениях, сочетающих прямой нагрев воздуха с регулируемым аккумулированием тепловой энергии. При этом особое значение приобретает разработка моделей, обладающих экспериментальной воспроизводимостью и верифицируемостью. Целью настоящей работы было формулирование и экспериментальное подтверждение оптико-теплотехнической модели интегрированного солнечного коллектора-аккумулятора с переменным углом раскрытия жалюзийного абсорбера. Модель описывает зависимость мгновенного коэффициента полезного действия (КПД) от плотности солнечного излучения при фиксированных углах открытия жалюзи – 0°, 45°, 60° и 90°, а также учитывает разделение поступающей энергии между воздушной ветвью и встроенным водяным теплоаккумулятором. На основе разработанного прототипа, заключенного в единый теплоизолированный корпус, были проведены стендовые испытания с регистрацией основных параметров: плотности солнечного потока, температур на входе и выходе воздушного канала, динамики нагрева воды и массового расхода воздуха. Математическая модель, лежащая в основе анализа, базировалась на балансе энергии с линейной зависимостью КПД от приведенной температуры, а идентификация параметров осуществлялась посредством метода наименьших квадратов. Динамика водяного звена описана через дифференциальное уравнение первого порядка. Надежность модели подтверждена высокими значениями доли объясненной дисперсии, отсутствием автокорреляции и соответствием распределения остатков нормальному закону. В работе представлены графические зависимости η (G) для четырех углов раскрытия жалюзи; при плотности солнечного потока 350, 650 и 1000 Вт/м^2 достигнута эффективность соответственно: ~0,36/0,50/0,56 для $\theta = 0°$, ~0,33/0,48/0,55 для $\theta = 45°$, ~0,32/0,47/0,54 для $\theta = 60°$, и ~0,30/0,45/0,50 для $\theta = 90°$. Усредненное значение КПД в диапазоне G = 200-1000 Вт/м^2 составило около 0,435. Показано, что умеренное увеличение угла открытия жалюзи до 45-60° приводит к снижению эффективности воздушной ветви на 1-4 процентных пункта, но, одновременно, способствует более активной зарядке водяного аккумулирующего звена. Совпадение модели с экспериментальными данными подтверждает ее практическую применимость и отсутствие систематической погрешности

Ключевые слова: жалюзийный абсорбер; солнечный поток; водяной аккумулятор; эффективность; инсоляция; эксперимент; управление углом